Electronic Supplementary Information

All-quantum dot based Förster resonant energy transfer: key parameters for high-efficiency biosensing

J. Hottechamps† · T. Noblet† · C. Méthivier ‡ · S. Boujday‡ · L. Dreesen†

† *GRASP-Biophotonics, CESAM, University of Liege, Institute of Physics, Allée du 6 Août 17, 4000 Liège, Belgium*

‡ *Sorbonne Universités, UPMC Univ. Paris 6, UMR CNRS 7197 Laboratoire de Réactivité de Surface, F75005 Paris, France*

Contents

1 Optical characterizations of QDs

1.1 Molar extinction coefficients and Förster radii

Figure 1 gives the molar extinction coefficients $\sigma(\lambda)$ of the four QD samples and their emission spectra. To compute the Förster radii of the five different QD-QD couples, we fit the fluorescence spectra by normalized Gaussian functions:

$$f(\lambda) = \frac{\exp\left[-\left(\frac{\lambda-\lambda_f}{\Delta\lambda}\right)^2\right]}{\Delta\lambda\sqrt{\pi}} \tag{S1}$$

and calculate the overlap integral J defined by:

$$J = \int \mathrm{d}\lambda \; f_D(\lambda)\,\sigma_A(\lambda)\,\lambda^4, \tag{S2}$$

where $f_D(\lambda)$ is the normalized Gaussian profile of the donor emission band and $\sigma_A(\lambda)$ the molar extinction coefficient of the acceptor. The Förster radius is then given by[2]:

$$\frac{R_0}{\mathrm{nm}} = 0.02108 \left(\frac{\kappa^2\phi}{n^4}\,\frac{J}{\mathrm{M}^{-1}\cdot\mathrm{cm}^{-1}\cdot\mathrm{nm}^4}\right)^{1/6}, \tag{S3}$$

where $\kappa = \sqrt{2/3}$ is the orientation factor, ϕ the quantum yield of the donor and $n = 1.33$ the refractive index of water. In the manuscript, the values of R_0 are gathered in Figure 3f.

When APTES is added to the colloidal suspensions, we notice a global increasing of the extinction coefficients (Figure S1). The effect of APTES is quite similar for the four samples. Quantitatively, we calculate the relative increasing of their extinction coefficients, defined as:

$$\frac{\Delta\sigma(\lambda)}{\sigma_{\mathrm{ex}}} = \frac{\sigma_{\mathrm{QD+APTES}}(\lambda) - \sigma_{\mathrm{QD}}(\lambda)}{\sigma_{\mathrm{QD}}(\lambda_{\mathrm{ex}})}, \tag{S4}$$

and displayed in Figure S1. We clearly observe the same behaviours: the APTES-related increasing of the extinction is characteristic of light scattering, consistent with QD aggregation. For QD1, which gives rise to the smallest QD clusters [3], $\frac{\Delta\sigma(\lambda)}{\sigma_{\mathrm{ex}}}$ can be fitted by a power law of type $A + B\cdot\lambda^n$ (Figure S1), with a parameter $n = -3.59$ close to the ideal value of -4. Hence, in terms of UV-visible response, the addition of APTES only leads to light scattering, without affecting the first excitonic peak and the intrinsic electronic structure of QDs (this, indifferently from a QD sample to another).

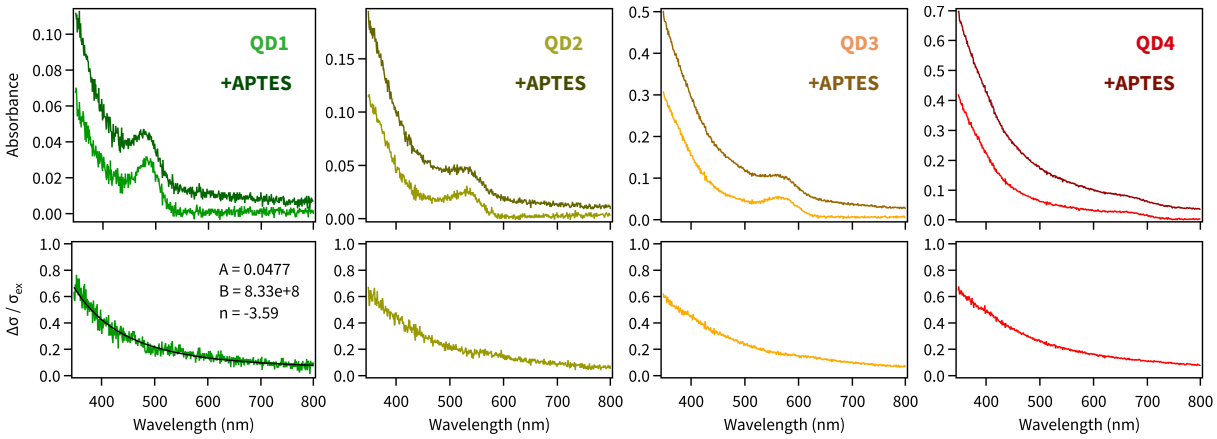

Figure S1: Top: UV-visible spectra of the four QD samples measured before (light colours) and after (dark colours) addition of APTES, for a QD concentration of 10^{-7} M. Bottom: Relative increasing of the corresponding extinction coefficients computed according to Eq. (S4). For QD1, the data are fitted by a power law of type $A + B\cdot\lambda^n$.

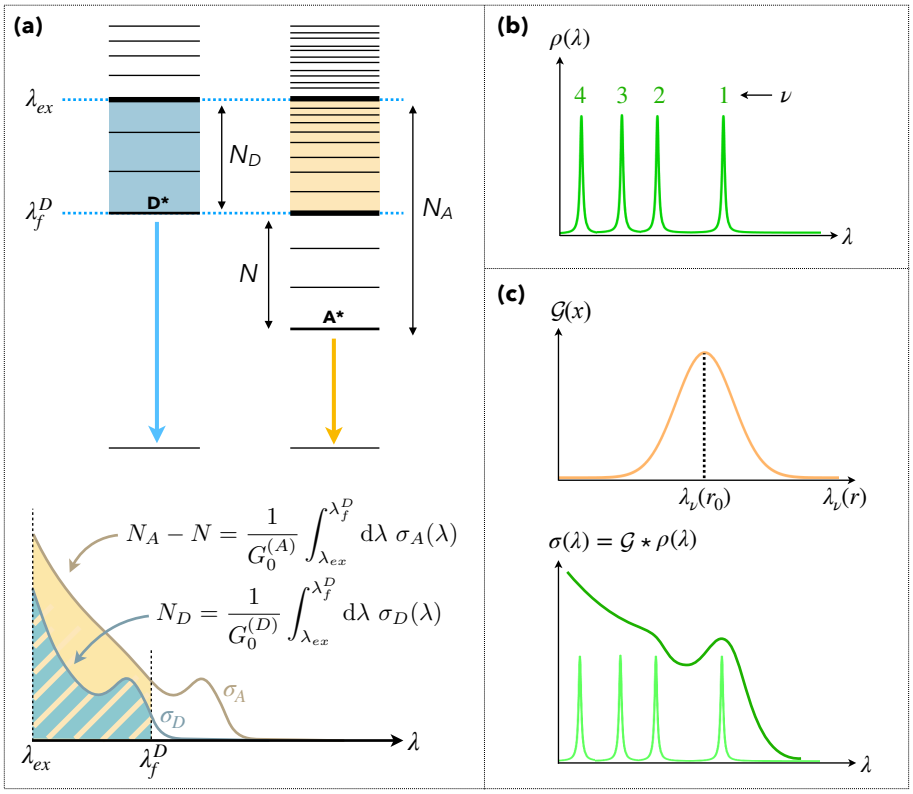

Figure S2: (a) Scheme of the energy diagrams of a QD donor and a QD acceptor (top) and the corresponding absorption spectra $\sigma_{D/A}(\lambda)$ (bottom). (b) Typical distribution of the excitonic states for a single QD. (c) Effect of the statistical distribution $\mathcal{G}(\lambda_\nu(r))$ of QD radii on the absorption spectrum $\sigma(\lambda)$ of a colloidal suspension.

1.2 Computation of parameter ΔN

In order to assess the numbers N_A, N_D and N of excitonic states implied throughout the cascade relaxation paths pictured in Figure 4, we assume that they are proportional to the areas under the curve of the corresponding absorption spectra (see Figure S2a). Indeed, as a first approximation, the absorption spectrum of a single QD is an image of its density of states. Given quantum confinement, this density of states is discrete (see Figure S2b). If $E_\nu(r)$ depicts the eigenenergy of the ν^{th} exciton of a QD of radius r, the QD absorption spectrum consists in a set of peaks located at the wavelengths:

$$\lambda_\nu(r) = \frac{hc}{E_\nu(r)}. \tag{S5}$$

Then, at the macroscopic scale of a colloidal suspension, the size distribution of the QDs (centered at the mean radius r_0) gives rise to a heterogeneous broadening of the absorption peaks (see Figure S2c). Each excitonic state ν is characterized by a Gaussian distribution $\mathcal{G}(\lambda_\nu(r) - \lambda_\nu(r_0))$, with:

$$\mathcal{G}(x) = \sigma_0 \exp\left[-\left(\frac{x}{\Delta\lambda}\right)^2\right], \tag{S6}$$

The resulting absorption spectrum $\sigma(\lambda)$ consists in the convolution product of the single-QD density of states $\rho(\lambda) = \sum_\nu \delta(\lambda - \lambda_\nu(r))$ and the Gaussian distribution of the QD radii:

$$\sigma(\lambda) = \sum_\nu \delta(\lambda - \lambda_\nu(r)) * \mathcal{G}(\lambda_\nu(r) - \lambda_\nu(r_0)) = \sum_\nu \mathcal{G}(\lambda - \lambda_\nu(r_0)). \tag{S7}$$

Assuming that each excitonic state ν follows the same dispersion (as encoded by Eq. (S6) wherein the amplitude σ_0 and the width $\Delta\lambda$ do not depend on ν), the Gaussian functions $\mathcal{G}(\lambda - \lambda_\nu(r_0))$ have all the same areas:

$$G_0 = \int \mathrm{d}x\ \mathcal{G}(x). \tag{S8}$$

Hence, from Eq. (S7):

$$\int_{\lambda_N(r_0)}^{\infty} \mathrm{d}\lambda\ \sigma(\lambda) = \sum_{\nu=1}^{N} \int \mathrm{d}x\ \mathcal{G}(x) = N \cdot G_0. \tag{S9}$$

As a result, we can deduce N from: (1) the computation of the area under the curve of the absorption spectrum until the wavelength of the N^{th} exciton; and (2) the knowledge of G_0. Figure S3 shows how the values of G_0 are estimated for the four samples. As illustrated in Figure S2a for a donor/acceptor couple, we thus obtain:

$$N_D = \frac{1}{G_0^{(D)}} \int_{\lambda_{ex}}^{\lambda_f^D} \mathrm{d}\lambda\ \sigma_D(\lambda) \quad \text{and} \quad N_A - N = \frac{1}{G_0^{(A)}} \int_{\lambda_{ex}}^{\lambda_f^D} \mathrm{d}\lambda\ \sigma_A(\lambda). \tag{S10}$$

The values of:

$$\Delta N = N_A - N - N_D \tag{S11}$$

are given in Figure 3f.

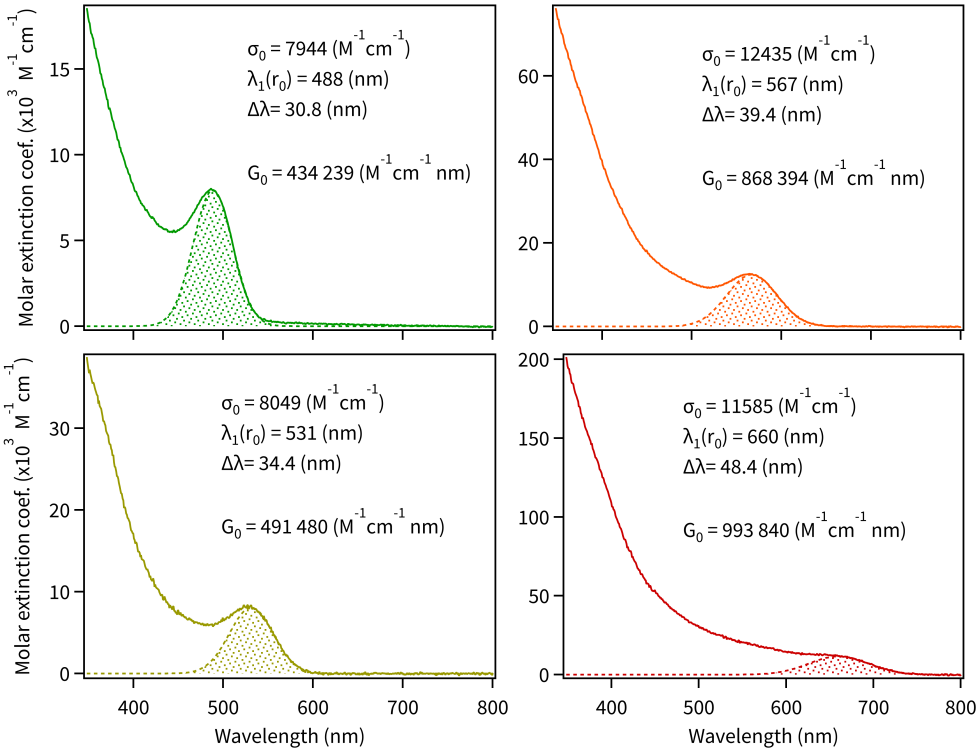

Figure S3: Molar extinction coefficients $\sigma(\lambda)$ of the four QD samples. The first absorption peak is fitted by a Gaussian function, from Eq. (S6). The quantity G_0 is the area of this band.

2 Experimental measurements of FRET efficiencies

In order to compute η_D and η_A, defined as:

$$\eta_D(x) = 1 - \frac{[D^*]}{[D^*_\circ]} \quad \text{and} \quad \eta_A(x) = \frac{[A^*]}{[A^*_\circ]} - 1, \tag{S12}$$

we fit the fluorescence spectra by Gaussian functions. For $[A^*_\circ]$ and $[D^*_\circ]$, the two QD populations are not mixed. We fit the respective spectra by single Gaussian functions, whose areas give the values of the fluorescence intensity $[A^*_\circ]$ and $[D^*_\circ]$. When the two QD populations are mixed, we fit the fluorescence spectrum of the mixture by a sum of two Gaussian functions. Their respective areas give the values of the intensities $[A^*]$ and $[D^*]$.

3 Characterizations of the QD ligands

3.1 XPS analysis

XPS measurements have been performed to estimate the chain lengths of the QD ligands. Figure S4 gives the spectra associated to the carbon content (1s state) of the four QD samples. We distinguish two XPS peaks associated to carbon atoms involved in $-\mathrm{COOH}$ and $-\mathrm{CH_2}-$ groups, respectively. Indeed, QDs are capped with mercaptocarboxylic acids:

$$\mathrm{HS}-(\mathrm{CH_2})_n-\mathrm{COOH}. \tag{S13}$$

Thus, the ratio ρ between the XPS signal of the COOH-related carbon atoms and that of the total amount of carbon (as given by the %Area indicated on Figure S4) is given by:

$$\rho = \frac{\#\mathrm{COOH}}{\#\mathrm{C}} = \frac{1}{1+n}. \tag{S14}$$

Hence:

$$n = \frac{1}{\rho} - 1. \tag{S15}$$

The values of n are given in Figure 3c.

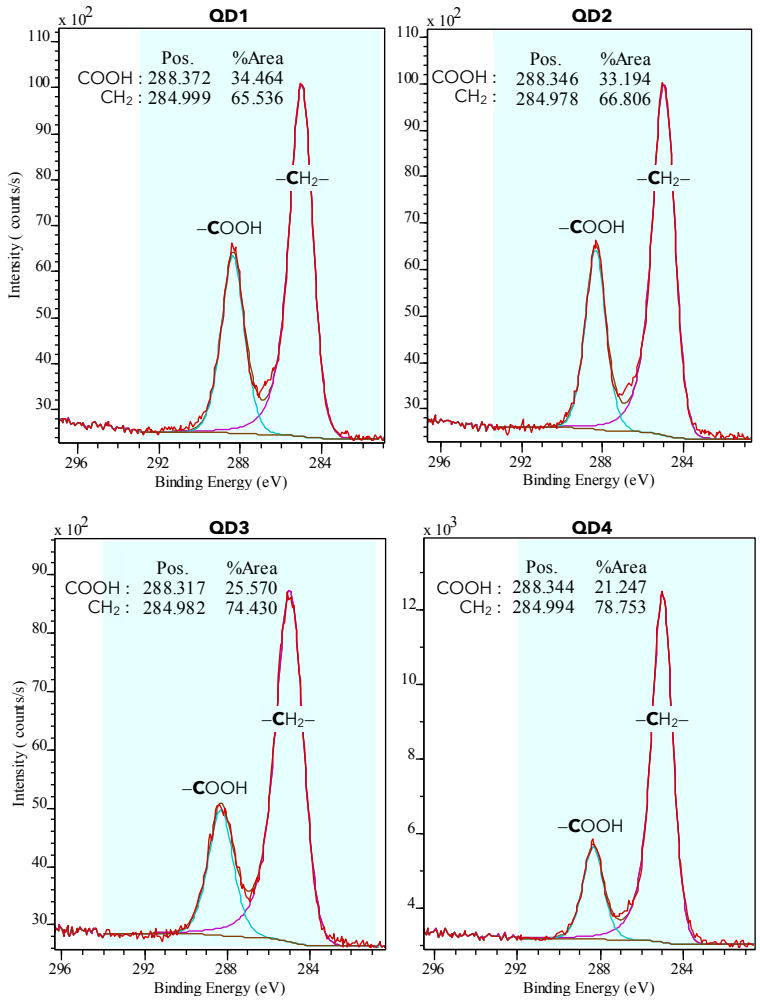

Figure S4: XPS spectra of the four samples QD1, QD2, QD3 and QD4 (deposited on silicon wafer) related to carbon (1s state). The energy positions and the relative areas of the peaks associated to COOH- and $\mathrm{CH_2}$-related carbon atoms are given. The ratio ρ defined by Eq. (S14) is deduced from the %Area of the COOH-related XPS peak.

3.2 Calculation of ligands' chain lengths

Thanks to the knowledge of their carbon numbers n, Eq. (S15), we can compute the lengths of the QD ligands, whose geometry is drawn in Figure S5. In our experimental conditions, the carboxylic groups are deprotonated and the electron is delocalized between the two oxygen atoms. Given the interatomic distances [1] gathered in the table of Figure S5, the ligand length reads:

$$L_{\mathrm{lig}}(n) = 126 \cdot n + 256 \quad \text{(pm)}. \tag{S16}$$

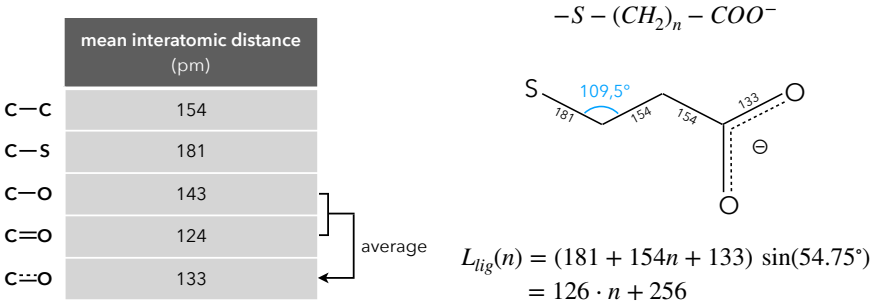

Figure S5: Left: Table gathering the mean values of the interatomic distances involved in the QD ligands, extracted from [1]. Right: Typical geometry of the QD ligands.

4 Mathematical derivations of FRET efficiencies

4.1 Fluorescence intensity of same-population QDs

We first consider a single monodisperse population of QDs aggregated by addition of APTES. Every QD experiences a molecular quenching due to APTES which translates into the existence of non-radiative relaxation paths, as modeled by the Jablonski-like diagram pictured in Figure S6. For a given QD named X, we call X^* its fluorescent state and N_X the rank of the excitonic state which coincides with the excitation wavelength. The lower excitonic states are then labelled by $n \in [\![1, N_X]\!]$. According to Figure S6, the rate equations are:

$$\frac{\mathrm{d}}{\mathrm{d}t}[N_X] = \sigma_{ex}^X \, \phi - (k_i + k_q)[N_X], \tag{S17}$$

$$\frac{\mathrm{d}}{\mathrm{d}t}[n] = k_i[n+1] - (k_i + k_q)[n], \qquad \text{for } 1 \leqslant n < N_X, \tag{S18}$$

$$\frac{\mathrm{d}}{\mathrm{d}t}[X^*] = k_i[1] - (k_r^X + k_{nr}^X)[X^*], \tag{S19}$$

where $[m]$ is the population of state $m \in \{X^*\} \cup [\![1, N_X]\!]$. The fluorescence intensity is thus proportional to $[X^*]$. Here, we assume multi-step relaxation paths in order to account for the fact that the probability of non-radiative relaxation increases with the number of states located between the excitation wavelength and the band gap emission, i.e. with N_X. Hence, k_i results from the combination of internal conversion (from an excitonic state $n+1$ to state n) and vibrational relaxation (within state n). The existence of a quenching process due to an external coupling with APTES is encoded by the rate constant k_q.

In steady-state regime, the time derivatives vanishes ($\frac{\mathrm{d}}{\mathrm{d}t}[m] = 0$), and we get:

$$[N_X] = \frac{\sigma_{ex}^X \, \phi}{k_i + k_q}, \tag{S20}$$

$$[n+1] = \left(1 + \frac{k_q}{k_i}\right)[n], \tag{S21}$$

$$[X^*] = \tau_X^\circ \, k_i \, [1], \tag{S22}$$

with:

$$\tau_X^\circ = \frac{1}{k_n^X + k_{nr}^X}. \tag{S23}$$

Equation (S21) is a geometric sequence which can be written:

$$[n+1] = \left(1 + \frac{k_q}{k_i}\right)^n [1], \qquad \text{for } 1 \leqslant n < N_X. \tag{S24}$$

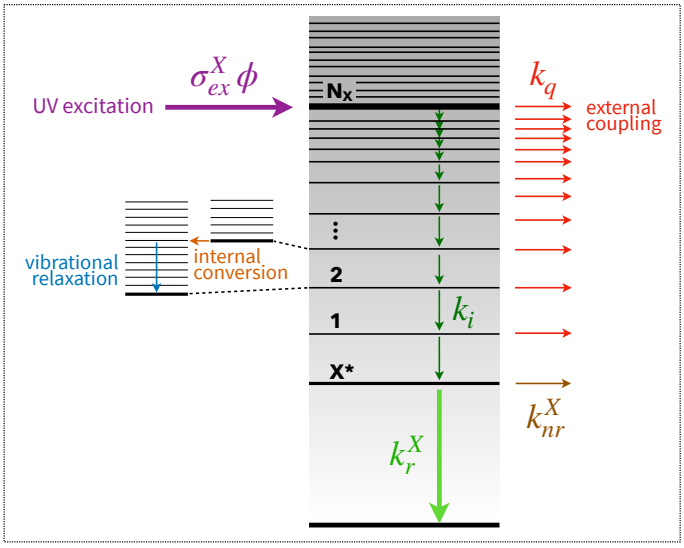

Figure S6: Model of energy diagram and relaxation paths of a QD in interaction with APTES.

Hence, for $n = N_X - 1$:

$$[N_X] = \left(1 + \frac{k_q}{k_i}\right)^{N_X - 1} [1]. \tag{S25}$$

As a result, from Eqs. (S20), (S22) and (S25), we obtain:

$$[X^*] = \tau_X^\circ \, \sigma_{ex}^X \, \phi \, (1 + \delta_k)^{-N_X} \,, \quad \text{with } \delta_k = \frac{k_q}{k_i}. \tag{S26}$$

4.2 Fluorescence intensities of a heterogeneous mix of QDs

We now consider a mix of two different monodisperse solutions of QDs. The APTES-mediated aggregation gives rise to hetero-FRET between the donor QDs of the first population and the acceptor QDs of the second one. Each FRET-active QD-QD couple is made of a donor D and an acceptor A. From Eq. (S26), the fluorescence intensities of each QD when there is no heterogeneous mix are given by:

$$[D_\circ^*] = \tau_D^\circ \, \sigma_{ex}^D \, \phi \, (1 + \delta_k)^{-N_D} \quad \text{and} \quad [A_\circ^*] = \tau_A^\circ \, \sigma_{ex}^A \, \phi \, (1 + \delta_k)^{-N_A}, \tag{S27}$$

according to the Jablonski-like diagram of Figure 4. When mixed and coupled, QDs follow new rate equations. For any donor D, we have:

$$\frac{\mathrm{d}}{\mathrm{d}t}[N_D] = \sigma_{ex}^D \, \phi - (k_i + k_q)[N_D], \tag{S28}$$

$$\frac{\mathrm{d}}{\mathrm{d}t}[n] = k_i[n+1] - (k_i + k_q)[n], \quad \text{for } 1 \leqslant n < N_D, \tag{S29}$$

$$\frac{\mathrm{d}}{\mathrm{d}t}[D^*] = k_i[1] - (k_r^D + k_{nr}^D + \mu(x) \, k_T)[D^*], \tag{S30}$$

where k_T is the particle-to-particle FRET rate constant and $\mu(x)$ is the number of acceptor QDs coupled to the donor D. In steady-state regime, this triplet of equations leads to:

$$[D^*] = \frac{\sigma_{ex}^D \, \phi \, (1 + \delta_k)^{-N_D}}{\mu(x) \, k_T + 1/\tau_D^\circ}. \tag{S31}$$

The donor-related FRET efficiency η_D is then given by:

$$\eta_D = 1 - \frac{[D^*]}{[D_\circ^*]} = \frac{\mu(x)}{\mu(x) + (r/R_0)^6}, \tag{S32}$$

wherein R_0 is the Förster radius and r is the D-A distance, related to k_T by:

$$k_T = \frac{1}{\tau_D^\circ} \left(\frac{R_0}{r}\right)^6. \tag{S33}$$

For any acceptor A, we get:

$$\frac{\mathrm{d}}{\mathrm{d}t}[N_A] = \sigma_{ex}^A \, \phi - (k_i + k_q)[N_A], \tag{S34}$$

$$\frac{\mathrm{d}}{\mathrm{d}t}[n] = k_i[n+1] - (k_i + k_q)[n], \quad \text{for } N < n < N_A, \tag{S35}$$

$$\frac{\mathrm{d}}{\mathrm{d}t}[N] = \nu(x) \, k_T[D^*] + k_i[N+1] - (k_i + k_q)[N], \tag{S36}$$

$$\frac{\mathrm{d}}{\mathrm{d}t}[n] = k_i[n+1] - (k_i + k_q)[n], \quad \text{for } 1 \leqslant n < N, \tag{S37}$$

$$\frac{\mathrm{d}}{\mathrm{d}t}[A^*] = k_i[1] - (k_r^A + k_{nr}^A)[A^*], \tag{S38}$$

where $\nu(x)$ is the number of donor QDs coupled to the acceptor A. In steady-state regime, it reads:

$$[N_A] = \frac{\sigma_{ex}^A \, \phi}{k_i + k_q}, \tag{S39}$$

$$[N_A] = (1 + \delta_k)^{N_A - N - 1}[N+1], \tag{S40}$$

$$[N] = \frac{\nu(x) \, k_T[D^*] + k_i[N+1]}{k_i + k_q}, \tag{S41}$$

$$[N] = (1 + \delta_k)^{N-1}[1], \tag{S42}$$

$$[A^*] = \tau_A^\circ \, k_i \, [1]. \tag{S43}$$

Given Eqs. (S31) and (S32), we obtain:

$$[A^*] = \tau_A^\circ \, (1+\delta_k)^{-N_A} \, \left(\frac{\nu(x)}{\mu(x)} \, \eta_D \, \sigma_{ex}^D \, (1+\delta_k)^{N_A - N_D - N} + \sigma_{ex}^A \right) \phi. \tag{S44}$$

The acceptor-related FRET efficiency η_A is then given by:

$$\eta_A = \frac{[A^*]}{[A_\circ^*]} - 1 = \eta_D \, \frac{\nu(x)}{\mu(x)} \, \frac{\sigma_{ex}^D}{\sigma_{ex}^A} \, (1+\delta_k)^{N_A - (N_D + N)} \, . \tag{S45}$$

4.3 Statistics of D-A couples

On a purely statistical point of view (i.e. without other physical considerations than geometry), the number of donors per acceptor (or acceptors per donor) follows a binomial distribution. For a given QD, if S is the number of FRET-available sites in its vicinity (i.e. the number of neighbours which are closed enough to perform FRET with it), the probability to have n donors amongst the S sites is:

$$P_D(n) = \binom{S}{n} \, p_D^n \, (1-p_D)^{S-n}, \tag{S46}$$

where p_D is the probability to draw a donor QD amongst the whole QD population (made of the mix of the two QD populations). Defining x as the donor-to-acceptor ratio of the mix:

$$p_D = \frac{x}{1+x}. \tag{S47}$$

Indeed, by definition of x, we count x donor QDs for 1 acceptor QD, i.e. for $(1+x)$ QDs. Conversely, the probability to have n acceptors amongst the S sites is:

$$P_A(n) = \binom{S}{n} \, p_A^n \, (1-p_A)^{S-n}, \quad \text{with} \quad p_A = \frac{1}{1+x}. \tag{S48}$$

As a result, the average number $\nu(x)$ of FRET-available donor QDs per acceptor is the expectation value of n within the probability distribution $P_D(n)$:

$$\nu(x) = S \cdot p_D = \frac{S\,x}{1+x}, \tag{S49}$$

and the average number $\mu(x)$ of FRET-available acceptor QDs per donor is the expectation value of n within the probability distribution $P_A(n)$:

$$\mu(x) = S \cdot p_A = \frac{S}{1+x}. \tag{S50}$$

We notice that $\nu(x) = x\,\mu(x)$ and, as expected, $\nu(\infty) = S$ and $\mu(\infty) = 0$.

All the physical and chemical behaviour of the APTES-assisted QD aggregation is hidden within the parameter S, which likely depends on the physicochemical interactions between QDs and APTES, the growth dynamics of the QD clusters, the repulsive electrostatic interactions between QDs and the size distributions of the two QD populations.

4.4 Expressions of the FRET efficiencies as functions of the D/A ratio

From Eqs. (S32) and (S50), the donor-related FRET efficiency reads:

$$\eta_D(x) = \frac{1}{1 + (r/R_0)^6 \cdot (1+x)/S}. \tag{S51}$$

Experimentally, S is the only unknown parameter. The Förster radius R_0 is computed from UV-Vis and fluorescence spectroscopies (section 1.1) and the D-A distance r is calculated as the sum of the QD radii (known from UV-Vis spectroscopy [3]) and the lengths of the QD ligands (from XPS measurements, section 2). Then, from Eqs. (S45) and (S49), the acceptor-related FRET efficiency is given by:

$$\eta_A(x) = \eta_D(x) \cdot x \cdot \frac{\sigma_{ex}^D}{\sigma_{ex}^A} \cdot \left(1 + \frac{k_q}{k_i} \right)^{N_A - (N_D + N)} . \tag{S52}$$

References

[1] P. Atkins, J. de Paula, and J. Keeler. *Atkins' Physical Chemistry*. Oxford University Press, 11 edition, 2018.

[2] I. Medintz and N. Hildebrandt. *FRET - Förster Resonance Energy Transfer*. Wiley-VCH, 2014.

[3] T. Noblet, J. Hottechamps, M. Erard, and L. Dreesen. Homogeneous Resonant Energy Transfer within Clusters of Monodisperse Colloidal Quantum Dots. *J. Phys. Chem. C*, 126:15309–15318, 2022.